Diese Arbeit wurde vorgelegt am
Institut für Technische Verbrennung (ITV)

Analysis of Spark Ignition Kernel Development and Early Flame Kernel Formation

Seminar: CES Seminar

Juni 2017

Vorgelegt von Presented by	Aleksandra Rezchikova Matrikelnummer: 341337 aleksandra.rezchikova@rwth-aachen.de
Prüfer Examiner	Tobias Falkenstein Institut für Technische Verbrennung (ITV) RWTH Aachen University

Contents

1 Motivation

In this work, the focus will lie on the flame initiation. A controlled spark ignition process, resulting in a successful flame propagation, is interesting not only for the fundamental combustion research, but its realization under lean conditions with a minimum energy deposition make this topic relevant for the development of efficient low-emission engines. A flame, resulting from a forced ignition will be explored further, because the widely used spark ignition engines fall in this category, and hence a premixed type of the flames.

A combustion is a process which involves a non-isothermal mixture of multiple species reacting through different chemical reactions. Navier Stokes equations are applicable for each specie k, which appear in the equations in the form of its mass fraction $Y_k = m_k/m$. Therefore, a computational effort grows with the number N of species presented in the applied chemical scheme, as the number of equations to solve increases (N is usually larger than 50 for most simple hydrocarbon fuels [10]). That makes the CFD of unsteady premixed flames with complex chemistry and transport, as it should be in case of the flame initiation, hard to perform.

Thus the actual goal is the development of flame initiation models, which describe flame propagation accurately and efficiently and cover the existence of unsteady flame transitions. In the scope of this seminar, the influence of early flame development parameters will be investigated and accounted for the flame speed evolution modeling. Finally, two different models are introduced, tested and compared with the experimental data.

2 Ideal Premixed Flames

A determination of the flame speed is the core element in the combustion theory. In the following, two definitions for flame speed will be used:

Absolute flame speed or Burning velocity s_L a velocity of the flame normal to the flame front and relative to the unburnt mixture;

Flame speed or Flame displacement speed s_d a propagation speed of the flame relative to the gas velocity on the unburned side $\vec{v}$.

These two velocities are related in the following manner:

$$s_d = s_L - \vec{v}_n \tag{1}$$

The burning velocity typically decreases with an increasing pressure but increases with an increasing temperature of the unburned gas.

2.1 Laminar Burning Velocity

In order to handle a real burning process of some fuel/oxidizer mixture, the most simple flame configuration should be discussed first. A common setting is the adiabatic one-dimensional planar steady premixed flame. The temperature, which the combustion products theoretically reach under such assumption of no energy loss, will be called adiabatic flame temperature T_{ad}.

The unstretched laminar burning velocity s_L^0, also called laminar flame speed, is a fundamental property of a given combustible mixture and is defined as a speed at which an unstretched laminar flame front will propagate through a quiescent, chemically-frozen mixture of unburned reactants.

2.1.1 Combustion Model

There are plenty of codes, which deal with one-dimensional laminar premixed flames. In this work,the FlameMaster code will be used, provided by the Institute for Combustion Technology RWTH Aachen University.

Just the knowledge of thermodynamic conditions, such as the temperature and pressure of unburned mixture, along with fuel and oxidizer types and their equivalence ratio $\phi = \frac{m_{fuel}/m_{ox}}{(m_{fuel}/m_{ox})_{st}}$ is not enough to compute a burning velocity. A chemical reaction mechanism and a transport model should also be provided.

Since the number of chemical parameters to introduce in a flame computation with complex chemistry can be counted in thousands, it is essential to know which of these parameters are really important to reduce a computational effort. For example, chemical scheme used in this work considers 682 species for burning n-Heptane/air mixture.

Transport models, which are used to calculate diffusion coefficients, viscosity and heat diffusion coefficients, also have a huge impact on flame speed evolution. The simulations using the same full chemistry but different transport models in [10] show how sensitive the calculations are, and that the assumption of equal diffusivities for all species does not lead to good results.

To ensure the correctness of data for s_L^0 from FlameMaster, it was compared to the experimental data taken from multiple sources (purple points in Figure 1). This shows the measurement uncertainty due to the effects of ignition, unsteadiness, compression and stretch. Moreover, two different transport models were compared, represented with green and blue lines. The transport model (blue), which takes into account also the different shape of species molecules, agrees better with experiments as expected and is thus taken for the further calculations.

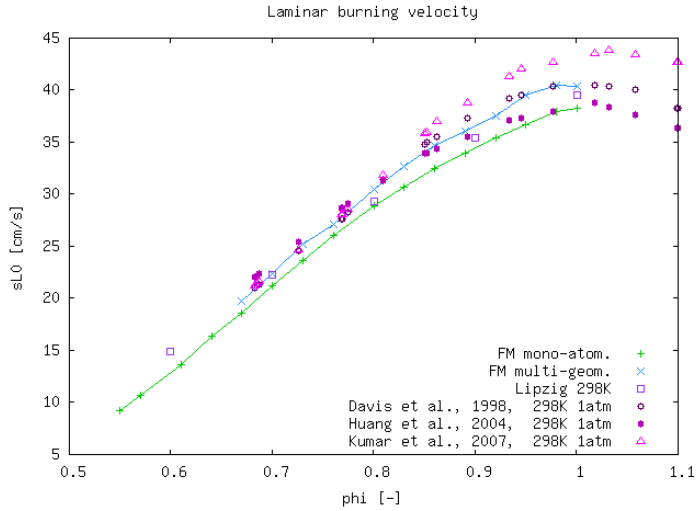

Figure 1: Flame propagation speed as function of equivalence ratio

3 Non-Ideal Premixed Flames

In reality the flames are multi-dimensional, stretched and unsteady. Their burning velocity is now a local property, generally unequal to s_L^0. The determination of s_L becomes tricky, since the mass flow rate varies through the flame.

3.1 Stretched Flames

Asymptotic studies, which treat the flame as thin, structured, internal layer, have shown for weakly stretched flames the linear dependence of the local flame displacement speed on the stretch rate $\mathcal{K}$:

$$s_d = s_L^0 - \mathcal{L}\mathcal{K} \tag{2}$$

where $\mathcal{L}$ is a proportionality coefficient, measuring a sensitivity of s_d to the stretch rate. $\mathcal{L}$ is usually hard to determine and it is known as the Markstein length. Empirically, a strong influence of the following quantities was established:

- $\sigma = \rho_u/\rho_b = T_b/T_u$ the expansion parameter;
- β Zel'dovich number;
- Le_{eff} effective Lewis number (will be defined below);
- $l_f = D_{th}/s_d$ diffusion length, a flame thickness characterization, where D_{th} is the thermal diffusivity;
- thermal conductivity λ_u.

The flame stretch $\mathcal{K}$ is a measure of surface deformation, defined as the Lagrangian time derivative of an element area, such that:

$$\mathcal{K} = \frac{1}{A}\frac{dA}{dt} \tag{3}$$

where A stands for the flame surface.

Matalon first proposed that the flame stretch is contributed by two sources: flame curvature $\kappa = \nabla \cdot \vec{n}$ and flow non-uniformity represented by hydrodynamic strain $K_s = -\vec{n} \cdot E \cdot \vec{n}$, with E being strain rate tensor.

$$\mathcal{K} = \kappa s_L^0 + K_s \tag{4}$$

The flame curvature contribution to the overall strain κs_L^0 results from a motion of a curved flame, whereas a hydrodynamic strain part is due to the straining by velocity gradients.

3.1.1 Spherical flames

As an example of a stretched flame may serve a spherical flame, what is usually the case when a combustible mixture is ignited at a point, like in spark engines. The products remains motionless due to the symmetry of spherical flames, and gas expansion drives the fresh mixture into a motion. In such flames the stretch is easily measured by measuring the changes of flame kernel radius as function of time $r_k(t)$.

$$\mathcal{K} = \frac{1}{A}\frac{dA}{dt} = \frac{2}{r_k}\frac{dr_k}{dt} \tag{5}$$

With the mass balance one obtains relation for flame displacement speed $s_d = \frac{1}{\sigma}\frac{dr_k}{dt}$. And using this for the stretch gives:

$$\mathcal{K} = \frac{2\dot{r_k}}{r_k} = \frac{2}{r_k}s_L^0 + \frac{\sigma - 1}{\sigma}\frac{2\dot{r_k}}{r_k} \tag{6}$$

3.2 Preferential Diffusion Effect

The term preferential diffusion will arise often in the further discussions and is enclosed in the definition of a Lewis number, a dimensionless number defined as the ratio of the thermal diffusivity to the mass diffusivity $Le = \frac{D_{th}}{D}$.

Le appears in a fluids characterization, where a simultaneous heat and mass transfer take place, like it is during combustion. But to characterize a combustible mixture, such that of fuel and air, an effective Lewis number should be introduced, defined as

an average value of the fuel and oxidizer Lewis numbers weighted more heavily with respect to the deficient component in the mixture [4]:

$$Le_{eff} = \begin{cases} \frac{Le_O + \mathcal{A} Le_F}{1+\mathcal{A}} & \phi < 1 \\ \frac{Le_F + \mathcal{A} Le_O}{1+\mathcal{A}} & \phi > 1 \end{cases} \tag{7}$$

$$\mathcal{A} = \begin{cases} 1 + \beta(\phi^{-1} - 1) & \phi < 1 \\ 1 + \beta(\phi - 1) & \phi > 1 \end{cases} \tag{8}$$

$Le_{eff} < 1$ indicates, that the mass diffusion is preferential, which enhance the overall burning rate, while $Le_{eff} > 1$ stands for the thermal preferential diffusion and add a negative correction to the overall burning rate.

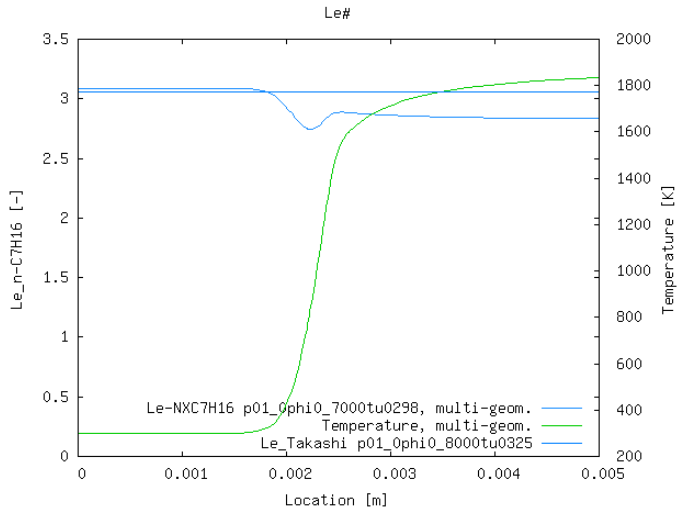

Figure 2: Lewis number and temperature change over the flame front

With the FlameMaster output one can also plot, how the mixture properties change through the flame, as it is done in Figure 2 for the Lewis number. Le does not change significantly through the flame, and its value on unburned side, which is usually used in speed calculations according to the theory [4], is in the correspondence with the values used in literature [11].

4 Flame Evolution

As the energy is deposited into a combustible mixture, a plasma channel is formed, causing a sudden, huge temperature and pressure increase, which in turn leads to an almost rectangular temperature profile at the contact interface between plasma and unburned mixture. These large gradients support the transport of a heat and a

mass from plasma to the fresh mixture and form a plasma kernel. When combustion reactions overcome the impact of kernel expansion, the plasma kernel turns into a flame kernel.

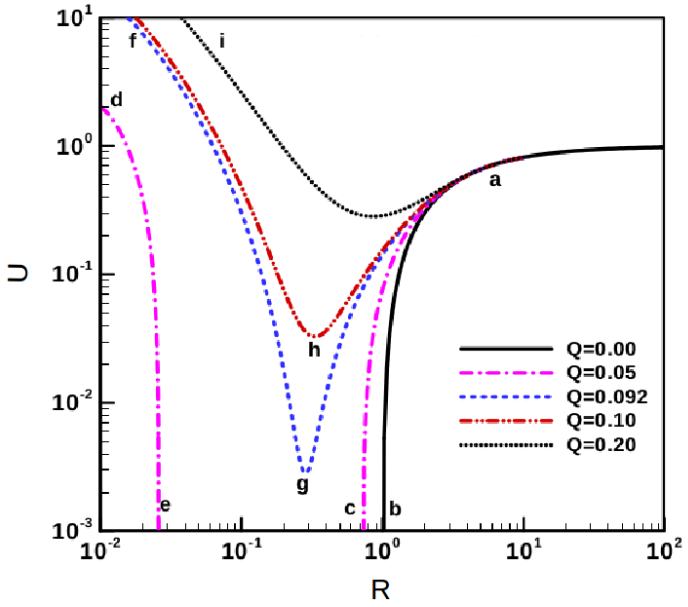

Figure 3: Normalized flame propagation speed versus normalized flame radius [2]

One can talk about successful ignition, if the expanding flame kernel is able to maintain its propagation to reach a self-propagating state. At this point the concept of minimum ignition energy (MIE) should be introduced and it is defined as the minimal critical ignition energy over which the ignition always succeeds. For example, in Figure 3, which is extensively discussed in [2], you can observe an evolution of the dimensionless flame propagating speed (normalized by its unstretched value) as function of kernel radius (normalized by the flame thickness) for different amounts of ignition energy. Without any external energy source a flame can propagate outward just in case when the initial flame kernel radius has a value which is more than one. For $Q = 0.05$, the initial flame kernel size for the initiation of a traveling flame decreases and a flame kernel branch $d - e$ appears, but this amount of energy is still not enough for a successful initiation of a self-propagating flame, as it quenches near point e. On this graph the MIE $Q = 0.092$ corresponds to the curve $f - g - a$ where flame kernel branch $f - g$ and traveling flame branch $g - a$ first merge. If more power will be deposited into the system, successful spherical flame initiation will be always achieved.

The determination of this MIE is an important task for the ignition control of internal combustion engines, since it defines whether the ignition will take place or fail due to the extinction of the ignition kernel. Therefore, this question was extensively studied and found in [2], that minimum ignition energy is directly proportional to the cube

of the so called critical flame radius(CFR). For this reason, a flame initiation model should take into account factors, which influence this radius.

CFR is independent of the ignition source and in Figure 3 located near the point a. It is important to differentiate critical flame radius from the critical ignition radius, which is the minimum point of the successful flame initiation curve. In contrast to CFR the critical ignition radius varies with the ignition power and also critical for successful ignition [6]. This leads to a conclusion, that a good flame initiation model should take into account possibly all factors, which influence CFR.

4.1 Flame Regimes

A general theory proposed the existence of different flame regimes for unsteady flame propagation and unsteady transitions among them. These regimes affect the flame initiation and define the value of CFR, thus they should be understood in detail and captured in the flame initiation modeling. As it discussed in [7], there are three such regimes:

Regime 1 spark assisted ignition kernel propagation;

Regime 2 unsteady transition from spark ignition to the outwardly propagating flame;

Regime 3 normal flame propagation.

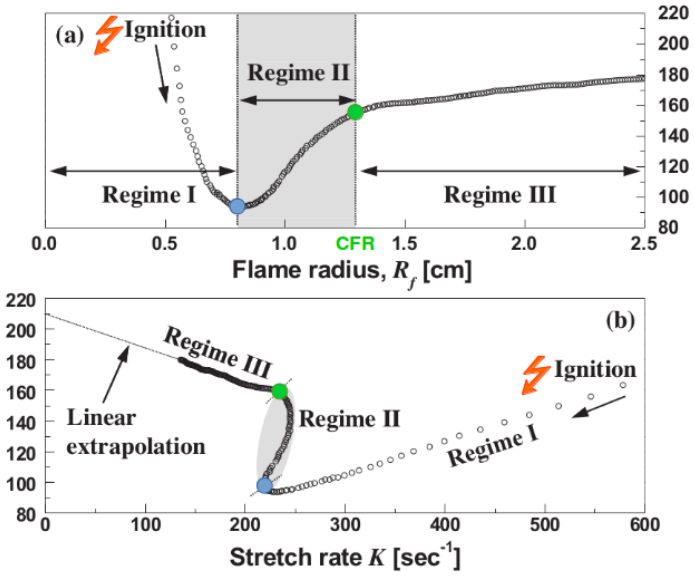

Figure 4: Regimes of unsteady flame propagation [7]

In Figure 4 a burning velocity evolution as function of flame radius and stretch rate is shown. The S-shaped stretch rate curve seen here, can be considered typical for high-hydrocarbon lean fuels. The first turning point (blue) on this curve is a transition between the first, and second regime, and correspond to the critical ignition radius. The second turning point (green) is the location of CFR and is determined as a transition between the second and the third regime.

After the critical flame radius is reached, the flame gets its normal structure and the flame kernel radius grows further, which leads to the stretch rate decrease. If these data will be extrapolated to the zero stretch values, the laminar flame speed can be determined.

In contrast to the third regime, the flame in the first one can be characterized as not self-sustained. Here, the kernel radius increases and hence the stretch rate goes down, at the same time the expansion rate decreases rapidly due to the spark energy dissipation. If the ignition energy overcome a MIE value, a transition from regime I to the normal flame arise in regime II. During the second regime, rapid flame speed increase together with rapid radius growth induce almost no difference in the stretch rate, but indicate a strong change in flame structure and chemistry. Namely, the flame thickness reduces and thus the diffusion of fuel accelerates, which leads to the flame temperature raise and consequently to the increase in radical pool concentration [7]. This big difference in the flame structure does not allow to extrapolate either linearly or nonlinearly the unstretched flame speed from the vicinity of first turning point.

4.2 Lewis Number Effect

As it was mentioned, Figure 4 correspond to the ignition process of lean large hydrocarbon fuels, which have high Le_{eff} values. The experimental results in Figure 5 show a strong dependence of flame stretch trajectories on the effective Lewis number.

In the case of small Lewis numbers (rich large hydrocarbon mixtures) the mass diffusion exceeds the thermal one. This mass diffusion leads to the flame stretch, which strengthens the flame propagation and decreases the critical flame radius. This positive correction to the overall burning rate prevents passing through the second regime and a flame progresses directly from regime I into regime II, that is why the S-shaped stretch curve is not longer seen for such mixtures. By big Lewis numbers the thermal diffusion dominates, leading to heat losses from the reaction zone. Since the CFR increases with Lewis number, the preferential diffusion effect plays an important role in the flame initiation.

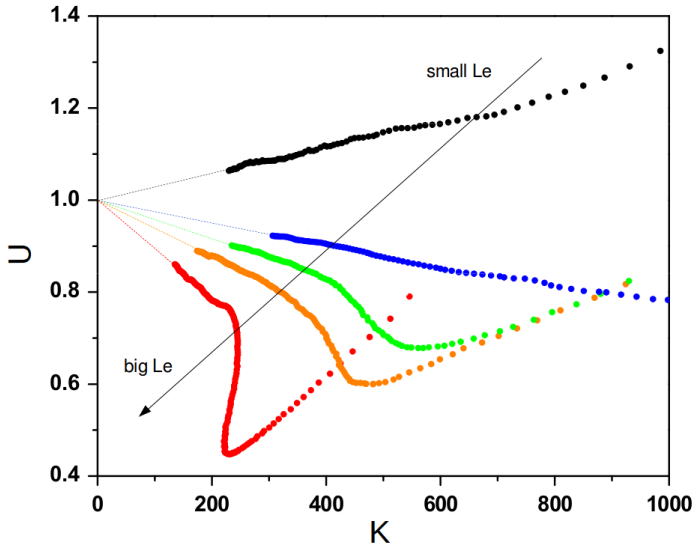

Figure 5: Normalized flame speed as function of stretch rate for different Le [7]

5 Modeling of Kernel Growth

In this section, two simplified flame initiation models will be introduced. The first one [1] (further called Matalon model for simplicity) was already implemented in the in-house code CIAO, a shortcut for Compressible Incompressible Advanced (Reactive Turbulent Simulation) with Overset grid. The second model, Chen model, an integral model developed by Zheng Chen, was implemented according to [3]. In both models an assumption of adiabatic conditions was made, excluding the effects of radiation heat loss.

5.1 Matalon Model

The existing model is part of a model framework "Spark Channel Ignition Monitoring Model" which has four distinct stages and discussed explicitly in [8]:

1. Electrical Circuit Modeling;
2. Spark Channel and Ignition Modeling;
3. Early Flame Kernel Development;
4. Turbulent Flame Propagation.

In this work, the second and third stages will be discussed, skipping the electrical circuit modeling and a transition to the turbulent flame. "Spark Channel and Ignition Modeling" includes the plasma heat conduction sub-model and thus the development of plasma kernel. A transition to the "Early Flame Kernel Development" was chosen

heuristically, as the kernel temperature falls to the value which is three times the adiabatic flame kernel temperature.

Since a plasma channel diameter is in the range of $50\mu m$, what is smaller than a commonly used LES grid size, each plasma channel particle is initiated as a Lagrangian particle of zero mass.

The heat conduction, imposed by the sudden huge gradients produced by the energy deposition (from $45000K$ to the temperature of unburned mixture), is developed using ADI (Alternating Direction Implicit Model) numerical scheme and fully described in [8]. The solution results in a plasma kernel ignition velocity s_{plasma}, which should correspond to velocities accounted for the regime I. In fact, this velocity should be understood not as the burning one, but as a traveling velocity of a steepest temperature gradient location.

As the temperature threshold is reached and transition to the third stage occurs, meaning the dominance of combustion reactions over the plasma induced expansion, s_{plasma} is added to the burning velocity s_f forming effective kernel growth speed s_{eff}.

On both stages the flame kernel growth is expressed by:

$$\frac{dm_k}{dt} = A_k \rho_u s_{eff} \tag{9}$$

where ρ_u represents the density of the unburned mixture, $A_k = 4\pi r_k^2$ is the surface area of the kernel with m_k and r_k being its mass and radius respectively.

The assumptions of ideal gas relations, of a negligible pressure increase due to the combustion and of a temperature uniformity inside a kernel, lead to the expression of its mean expansion velocity:

$$\frac{dr_k}{dt} = \frac{\rho_u}{\rho_k} s_{eff} \tag{10}$$

In the simulation set-up we also neglect a heat loss to spark plug electrodes, that reduces the equation for temperature to:

$$\frac{dT_k}{dt} = -\frac{\dot{m}_k}{m_k}(T_k - T_{ad}) + \frac{\dot{Q}_{spk}}{m_k c_p} \tag{11}$$

where $\dot{Q}_{spk}$ stands for rate of energy supply from spark, computed on the "Electrical Circuit Modeling" stage. T_k is here a temperature within the kernel and T_{ad} is the adiabatic flame temperature from FlameMaster.

This model utilizes the asymptotic theory of weakly stretched flames in calculating s_f, proposed by Matalon, which relates local flame speed with the flame stretch in a way it was written earlier.

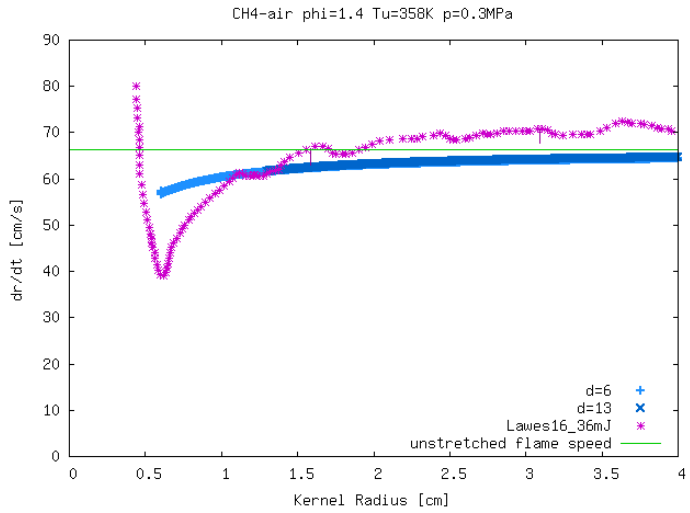

Figure 6: Flame displacement speed as function of kernel radius without plasma conduction.

The simulation results for the flame, that was initialized as a hot pocket of a radius, corresponding to the first and second turning points, skipping the plasma conduction phase, are demonstrated in Figure 6 and compared to the experimental results from [9].

This implementation predicts the flame speed relatively good in the region III. In this segment, the flame stretch influence is weak. As the kernel radius increases, the flame speed approaches the zero-stretched value from the combustion model, represented with a green horizontal line. But the speed is over-predicted in regime II, because the flame in this region is still highly stretched, which cannot be captured with a theory of weakly stretched flames.

When a plasma conduction phase is included in another setup, meaning the addition of s_{plasma}, a general flame over-prediction is observed, and flame speed approaches its unstretched value from above, which does not correctly reflect the reality. The results of this setup are demonstrated in Figure 7.

The application of this model is restricted to regime III, since a simple summation of the burning velocity obtained with the theory of weakly stretched flames with the plasma induced component cannot predict regime II.

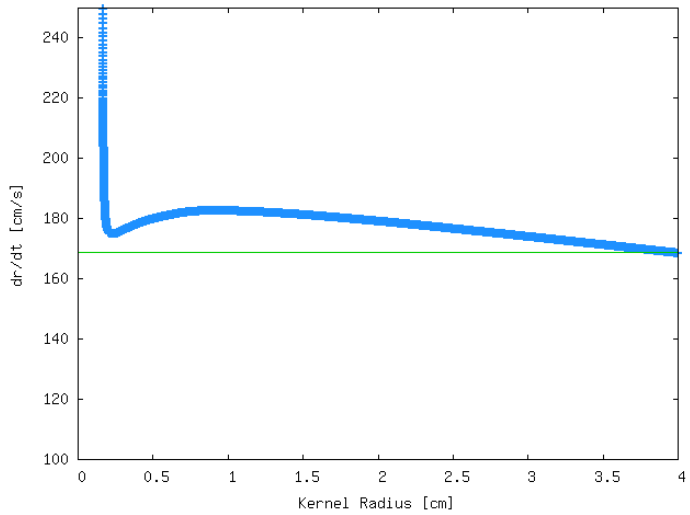

Figure 7: Flame displacement speed as function of kernel radius

5.2 Chen Model

An integral model introduced by Zheng Chen in [3] was implemented assuming the following simplifications:

- energy deposition is a boundary condition, independent of time and space;
- one-step irreversible reaction;
- thin reaction zone;
- constant thermodynamic and transport properties;
- quasi-steadiness by attaching the coordinate to the moving flame front;

Its derivation starts from two equations for an unsteady spherical flame kernel evolution: one for the mixture temperature and one for the fuel mass fraction, which are related with jump conditions at the flame interface. The usage of this model is limited just to lean cases, due to the choice of boundary conditions. As a result, the following system of algebraic equations arises, which is solved by the means of Newton's method with an adjusted damping factor.

$$\frac{T_k R^{-2} e^{-UR}}{\int_R^\infty \tau^{-2} e^{-U\tau} d\tau} - QR^{-2}e^{-UR} = \frac{1}{Le}\frac{R^{-2}e^{-ULeR}}{\int_R^\infty \tau^{-2}e^{-U\tau}d\tau}d\tau = exp\left[\frac{\beta}{2}\frac{T_k - 1}{\frac{1}{\sigma} + (1-\frac{1}{\sigma})T_k}\right] \tag{12}$$

All variables appear in their dimensionless form with $R(t)$ being a kernel radius, β the Zel'dovich number, Le the Lewis number of fuel, $U(t) = \frac{R(t)}{dt}$ the speed of the flame front, normalized by its unstretched value. More details regarding the derivation can be found in the dissertation of Chen [2].

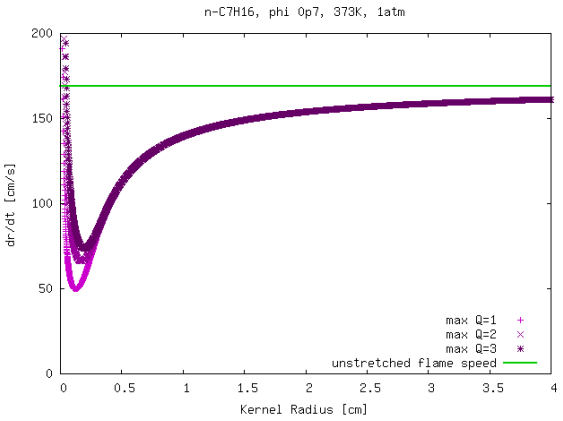

Figure 8: $\dot{r}_k$ as function of r_k for different Q

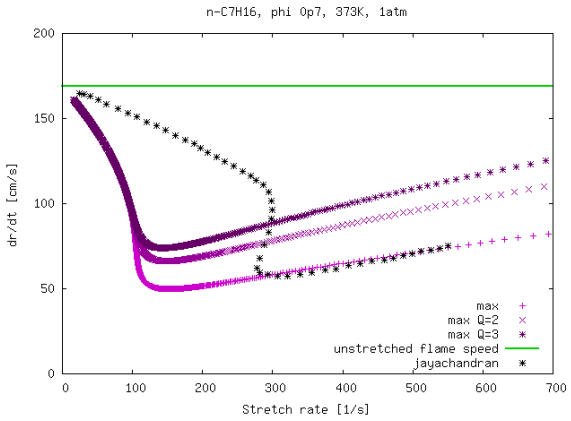

Figure 9: $\dot{r}_k$ as function of $\mathcal{K}$ for different Q

The impact of the ignition energy may be demonstrated by varying its amount, as it is shown in Figures 8 and 9. The experimental results for the stretch rate data are represented with the black points. It was measured by Jayachandran and discussed in [5]. The model results reflect the reality qualitatively, as the position of the second turning point, corresponding to the transition to the normal flame, remains unchanged, whereas the critical ignition radius increases with the deposited energy. However, the correct shape of stretch curve was not attained.

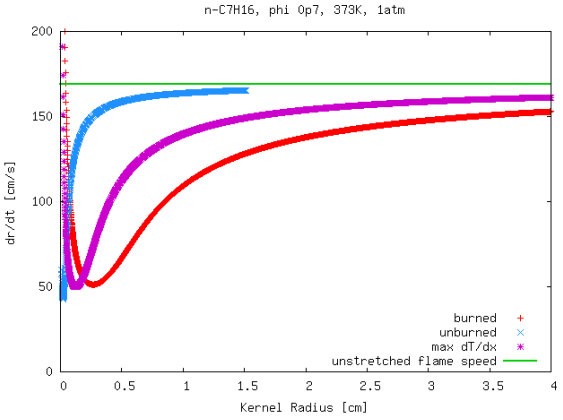

Figure 10: $\dot{r}_k$ as function of r_k for different properties

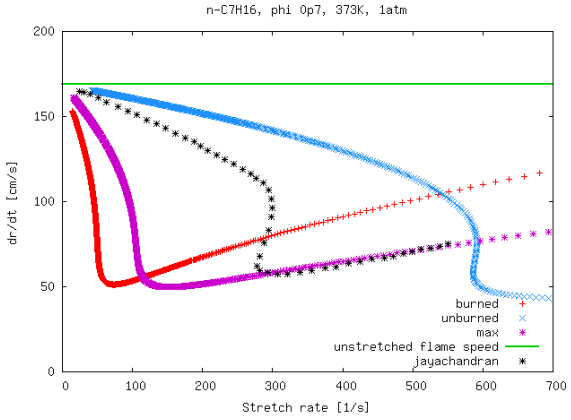

Figure 11: $\dot{r}_k$ as function of $\mathcal{K}$ for different properties

Figures 10 and 11 show how strong the assumption of constant properties. The properties were determined for unburned temperature T_u (blue line), for burned T_b (red) and for the value, corresponding to the maximum temperature gradient $T_{\frac{dT}{dr}\big|_{max}}$ (purple). These were provided as the input parameters. None of these choices coincide

with the experimental data, but the shape of the stretch curve for T_u is similar to the experimental, just shifted on the right.

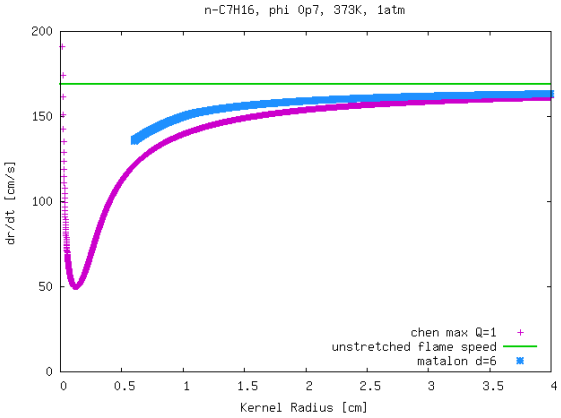

Figure 12: $\dot{r}_k$ as function of r_k for both models

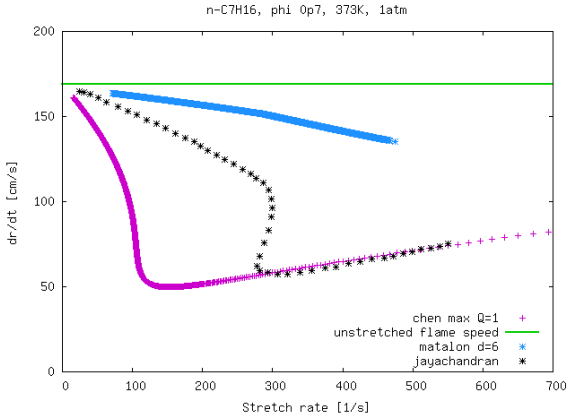

Figure 13: $\dot{r}_k$ as function of $\mathcal{K}$ for both models

In the next two Figures 12 and 13, results obtained from the Chen model (purple) and from the Matalon model (blue) are compared to the experimental data. Although both models tend to correctly predict the velocities for large radii (small stretch values), they fail to provide a correct shape of the stretch curve.

6 Conclusions

The models discussed above provide a good qualitative description of the most important features, but do not produce quantitative results.

The next step may be development of a new model, which is capable of capturing the different impact of the flame chemistry on its initiation. Other alternative is the conduction of exact one-dimensional calculations for laminar unsteady spherical flames with a detailed reaction mechanism and multi-species transport models. Those results may be tabulated and then used in CFD simulations.

References

[1] J.K. Bechtold and M. Matalon. The dependence of the markstein length on stoichiometry. *Combustion and Flame*, 127:1906–1913, 2001.

[2] Z. Chen. *Studies on the Initiation, Propagation, and Extinction of Premixed Flames*. PhD thesis, Princeton University, 2009.

[3] Z. Chen and Y. Ju. Theoretical analysis of the evolution from ignition kernel to flame ball and planar flame. *Combustion Theory and Modelling*, 11:3:427–453, 2007.

[4] G. K. Giannakopoulos, A. Gatzoulis, C. E. Frouzakis, M. Matalon, and A. G. Tomboulides. Consistent definitions of "flame displacement speed" and "markstein length" for premixed flame propagation. *Combustion and Flame*, 162:1249–1264, 2015.

[5] J. Jayachandran, A. Lefebvre, R. Zhao, F. Halter, E. Varea, B. Renou, and F. N. Egolfopoulos. A study of propagation of spherically expanding and counterflow laminar flames using direct measurements and numerical simulations. *Proceedings of the Combustion Institute*, 35:695–702, 2015.

[6] A. P. Kelley. *Dynamics of Expanding Flames*. PhD thesis, Princeton University, 2011.

[7] H. H. Kim, S. H. Won, J. Santner, Z. Chen, and Y. Ju. Measurements of the critical initiation radius and unsteady propagation of n-decane/air premixed flames. *Proceedings of the Combustion Institute*, 34:929–936, 2013.

[8] R. Lakshmanan. Large-eddy simulation of spark ignition and flame kernel development at engine-relevant conditions. Master's thesis, Institute for Combustion Technology RWTH Aachen University, 2015.

[9] M. Lawes, G.J. Sharpe, N. Tripathi, and R.F. Cracknell. Influence of spark ignition in the determination of markstein lengths using spherically expanding flames. *Fuel*, 186:579–586, 2016.

[10] T. Poinsot and D. Veynante. *Theoretical and Numerical Combustion*. Edwards, 2005.

[11] H. Takashi and T. Kimitoshi. Laminar flame speeds of ethanol, n-heptane, iso octane air mixtures. *F2006SC40*, 2006.